JACS
JOURNAL OF THE AMERICAN CHEMICAL SOCIETY

Solution-Phase Mechanistic Study and Solid-State Structure of a Tris(Bipyridinium Radical Cation) Inclusion Complex

Albert C. Fahrenbach,[1,5] Jonathan C. Barnes,[1,5] Don Antoine Lanfranchi,[2] Hao Li,[1] Ali Coskun,[1,5]

Jeremiah J. Gassensmith,[1] Zhichang Liu,[1] Diego Benítez,[3] Ali Trabolsi,[1,4]

William A. Goddard III,[3,5] Mourad Elhabiri[2]*, J. Fraser Stoddart[1,5]*

[1]*Department of Chemistry, Northwestern University, 2145 Sheridan Road, Evanston, Illinois 60208-3113 (USA)*
[2]*Laboratoire de Chimie Médicinale et Bioorganique, UMR 7509 CNRS-UdS, ECPM, Université de Strasbourg, 25, rue Becquerel, 67200 Strasbourg (France)*
[3]*Materials and Process Simulation Center, California Institute of Technology, Pasadena, California 91125, USA*
[4]*New York University Abu Dhabi, Center for Science and Engineering, Abu Dhabi (UAE)*
[5]*NanoCentury KAIST Institute and Graduate School of EEWS (WCU), Advanced Institute of Science and Technology (KAIST), 373-1, Guseong Dong, Yuseong Gu, Daejeon 305-701, Republic of Korea.*
*E-mail:stoddart@northwestern.edu

SUPPORTING INFORMATION - REVISED

* Correspondence Address	
Professor J Fraser Stoddart Department of Chemistry Northwestern University 2145 Sheridan Road Evanston, Illinois 60208-3113 Tel: (+1)-847-491-3793 Fax: (+1)-847-491-1009 E-Mail: stoddart@northwestern.edu	Dr Mourad Elhabiri Laboratoire de Chimie Médicinale et Bioorganique (UMR 7509 CNRS-UdS), ECPM, Université de Strasbourg, 25 rue Becquerel, 67200, Strasbourg, France. Tel: (+33)-368 852 685 Email: elhabiri@chimie.u-strasbg.fr,

1. General Methods

The tetracationic cyclophane cyclobis(paraquat-*p*-phenylene) tetrakishexaflourophosphate[S1] (CBPQT•4PF_6), the dimethyl viologen[S2] MV•2PF_6, the dibutynyl viologen[S3] V•2PF_6 and the single-station [2]rotaxane[S4] R•6PF_6 were prepared according to literature procedures. Zinc dust was activated by stirring with dilute HCl during 10-15 minutes, and then washed several times with distilled H_2O, EtOH and absolute Et_2O before rigorous drying. This procedure removes oxides from the surface of zinc, which form slowly upon standing in air.[S5] All the studies were carried out with spectroscopic grade MeCN (Acros Organics ≥ 99.9% for spectroscopy). All the stock solutions of CBPQT•4PF_6 and MV•2PF_6 were prepared by weighing using an AG 245 Mettler Toledo analytical balance (precision 0.01 mg) and complete dissolution in MeCN was achieved using an ultrasonic bath (Bandelin Sonorex RK102 Transistor). Thus, their concentrations were obtained by weighing the appropriate amounts. Reduction of $CBPQT^{4+}$ and MV^{2+} into the corresponding bisradical $CBPQT^{2(\bullet+)}$ and monoradical $MV^{+\bullet}$ was achieved under argon (CO_2- and O_2-free argon using a Sigma Oxiclear cartridge) in less than 1 h by vigorous stirring with activated zinc dust, while being monitored (Figures S1 and S2) by absorption spectrophotometry. Nuclear magnetic resonance (NMR) spectra were recorded at 298 K on a Bruker Avance 600 spectrometer with a working frequency of 600 MHz for ^1H. Chemical shifts are reported in ppm relative to the signal corresponding to the residual non-deuterated solvent (CD_3CN: δ 1.94 ppm). Isothermal titration calorimetry (ITC) experiments were performed on a MicroCal system, VP-ITC model. Cyclic voltammetry (CV) was carried out at room temperature in argon-purged solutions in MeCN with a Gamry Multipurpose instrument (Reference 600) interfaced to a PC. CV was performed using a glassy carbon working electrode (0.071 cm^2, BASi). The electrode surface was polished routinely with 0.05 μm alumina-water

slurry on a felt surface immediately before use. The counter electrode was a Pt coil and the reference electrode was a Ag/AgCl electrode unless otherwise noted. The concentration of the sample and supporting electrolyte, tetrabutylammonium hexafluorophosphate (TBA•PF_6), were 1.0×10^{-3} mol L^{-1} and 0.1 mol L^{-1}, respectively. Experimental errors: potential values, +/– 10 mV. All simulations of electrochemical data were performed using DigiSim.

2. ^{1}H NMR DOSY

In order to measure the diffusion coefficients of the $CBPQT^{4+}$ ring and MV^{2+} to use in digital simulations of the CV data, ^{1}H NMR diffusion-ordered spectroscopy (DOSY) was carried out on solutions of CBPQT•4PF_6 and MV•2PF_6 in CD_3CN at 1 mM concentrations. The results reveal that the diffusion coefficient (D_o) for the $CBPQT^{4+}$ ring is 2.82•10^{-5} cm^2 s^{-1}, and for MV^{2+}, 3.98•10^{-5} cm^2 s^{-1}. In the digital simulations we assumed that the radical cation and neutral forms of $CBPQT^{4+}$ and MV^{2+} have the same values of D_o, and that the trisradical complex $CBPQT^{2(\bullet+)}\subset MV^{\bullet+}$ has a D_o value similar to that of $CBPQT^{4+}$.

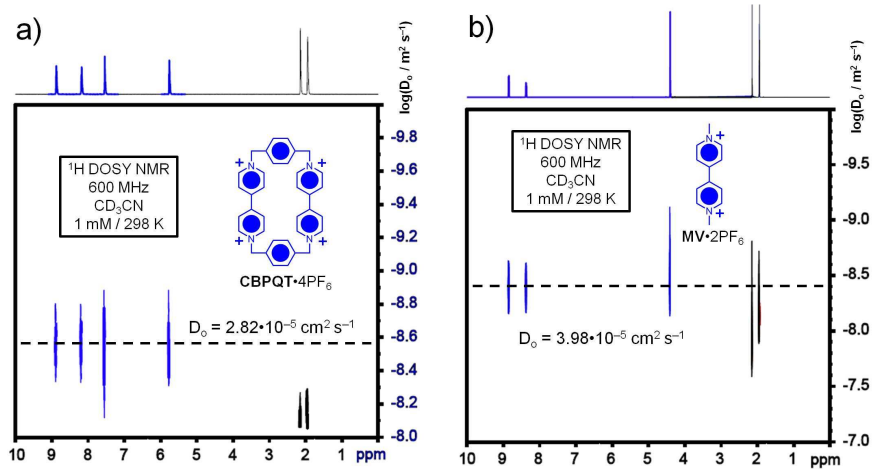

Figure S1. ^{1}H DOSY NMR of a) the $CBPQT^{4+}$ ring and b) MV^{2+}. The diffusion coefficients obtained were applied to the digital simulation studies. Each 2D DOSY was acquired in CD_3CN at 298 K.

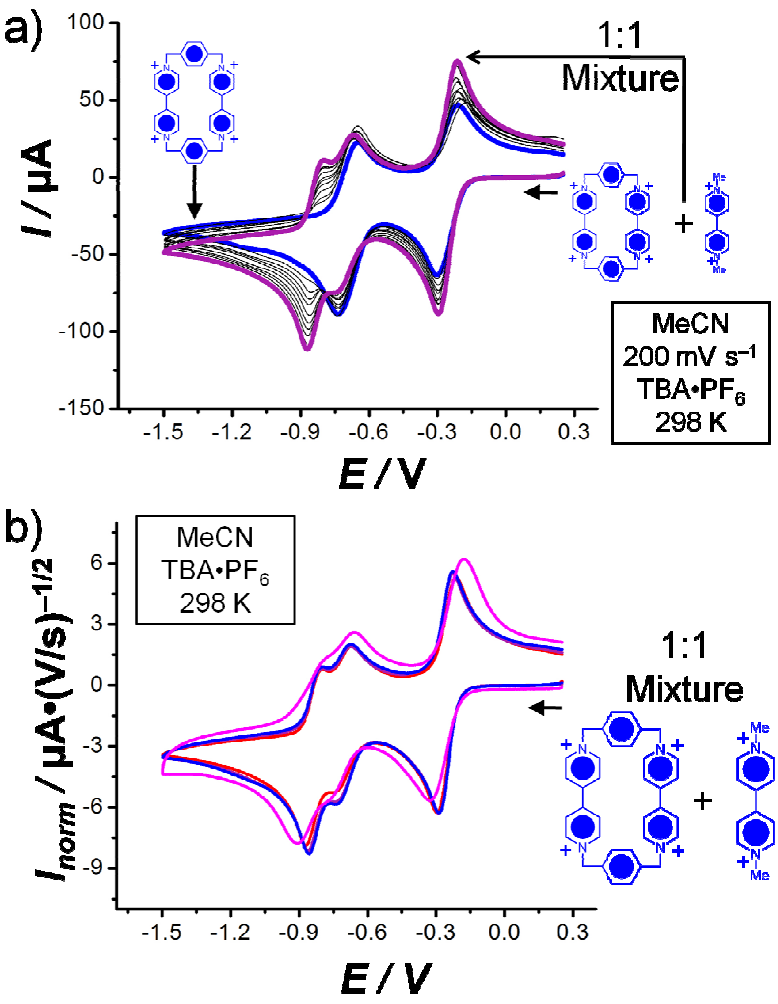

Figure S2. a) A CV titration of a solution of MV^{2+} (10 mM) into a solution of $CBPQT^{4+}$ (1.0 mM) in MeCN at 298 K. Blue trace: $CBPQT^{4+}$ only. Purple trace: 1:1 mixture of $CBPQT^{4+}$ and MV^{2+}. b) Variable scan rate CVs of the 1:1 mixture of $CBPQT^{4+}$ and MV^{2+} in MeCN at 298 K. Blue trace: 200 mV s^{-1}; red trace: 1000 mV s^{-1}; pink trace: 30 V s^{-1}.

3. Electrochemistry

Figure S2a shows a CV titration of MV^{2+} into a 1 mM solution of $CBPQT^{4+}$ in MeCN at 298 K. As more MV^{2+} is titrated into the solution of $CBPQT^{4+}$, a new redox process is observed to grow in at approximately −0.85 V. These observations provide evidence for the formation of the trisradical $CBPQT^{2(\bullet+)}\subset MV^{\bullet+}$, after the first three-electron reduction process. Figure S3b shows the variable scan rate CV data recorded on the 1:1 mixture of $CBPQT^{4+}$ and MV^{2+}. No significant changes are observed on scanning up to a rate of 30 V s^{-1}, an observation which implies that the bisradical $CBPQT^{(2+)(\bullet+)}\subset MV^{\bullet+}$ complex dissociates at a rate greater than 5000 s^{-1} M^{-1} by comparison with CV data simulated digitally.

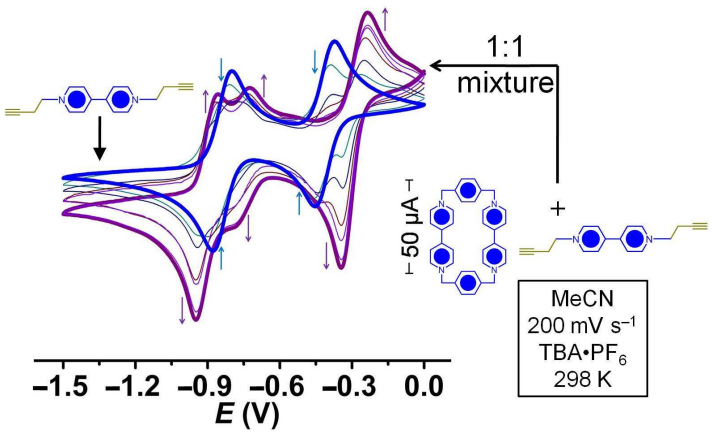

Figure S3. A CV titration of $CBPQT^{4+}$ (10 mM) into a solution of V^{2+} (1 mM) in MeCN at 298 K. Blue trace: V^{2+} only. Purple trace: 1:1 mixture of $CBPQT^{4+}$ and V^{2+}.

Figure S3 shows a CV titration starting with MV^{2+} (thick blue trace) and adding up to 1 equiv of the $CBPQT^{4+}$ ring (thick purple trace). The two reversible one-electron redox processes resulting from MV^{2+} alone decrease (blue arrows) as more $CBPQT^{4+}$ is added to the solution, resulting in the growth of three new anodic and cathodic peaks (purple arrows), an observation which is indicative of a new species being generated in solution upon reduction.

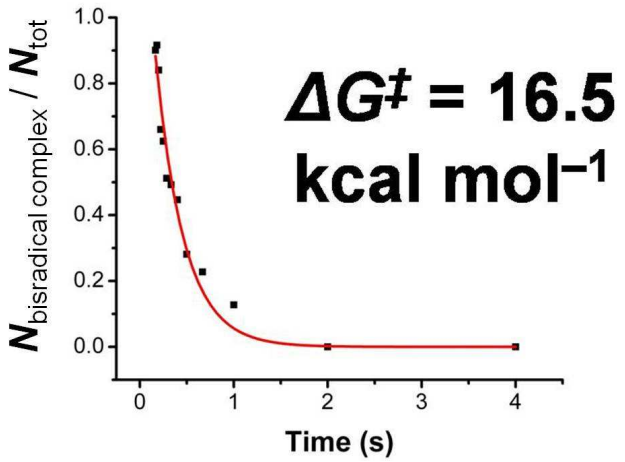

Figure S4. Relative integration analysis of the dissociation of the bisradical complex $CBPQT^{(2+)(\bullet+)}\subset V^{\bullet+}$ into its free components based on variable scan rate CV data shown in the maintext.

Quantification of the amount of the re-oxidation peak as a function of scan rate can be accomplished through relative integration, taking into consideration the fact that the first re-oxidation peak is a one-electron process, while the second one is a two-electron process. The relative integration approaches a 1:2 ratio at increasingly faster scan rates. At approximately 10 V s^{-1}, the relative integration is 1:2 and this ratio does not change upon

transition to higher scan rates, an observation which indicates that the second oxidation is truly a two-electron process and that virtually no dissociation occurs on time scales less than 10 V s^{-1}. Since the relative integration represents the relative amount of bisradical complex to that which has dissociated after the first one-electron oxidation, plotting this integration against time reveals a decay profile. Fitting this data to a first-order decay profile and extracting a rate constant to use in the Eyring equation reveals (Figure S4) this decay (or relaxation) process to be governed by a barrier of 16.5 kcal mol^{-1}.

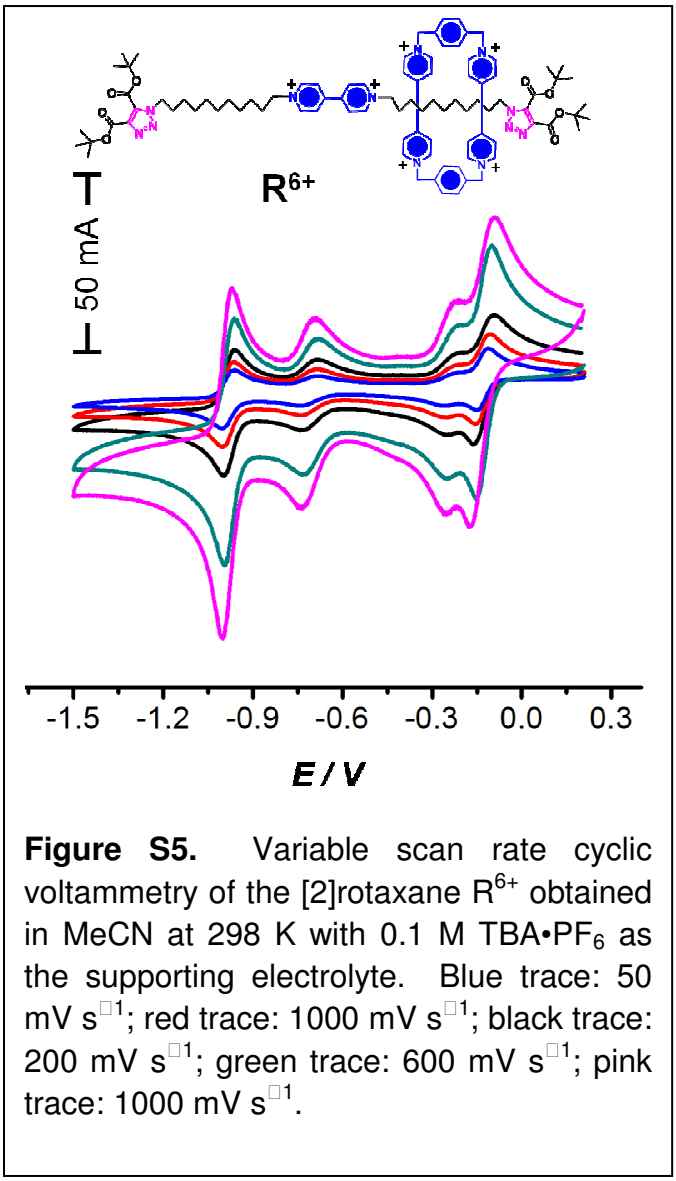

Figure S5. Variable scan rate cyclic voltammetry of the [2]rotaxane R^{6+} obtained in MeCN at 298 K with 0.1 M TBA•PF_6 as the supporting electrolyte. Blue trace: 50 mV s^{-1}; red trace: 1000 mV s^{-1}; black trace: 200 mV s^{-1}; green trace: 600 mV s^{-1}; pink trace: 1000 mV s^{-1}.

In the absence of π-electron-rich units in the dumbbell component, as is the case in the [2]rotaxane R^{6+}, no scan-rate dependent behavior is observed in the CV (Figure S5), and all four redox processes are totally reversible. The CV in the reductive region of the rotaxane shows first-of-all two reduction processes, corresponding to one- and two-electron processes; one after the other. Compared to the free $CBPQT^{4+}$ ring and the free dumbbell individually in solution, these potentials are shifted quite substantially to more positive values. The first reduction peak is assigned to the simultaneous reduction of one of the $BIPY^{\bullet+}$ radical

cations in the $CBPQT^{2(\bullet+)}$ ring and the one present in the dumbbell component. The second one-electron process observed is assigned to the remaining unpaired $BIPY^{\bullet+}$ of the $CBPQT^{(2+)(\bullet+)}$ ring component. These results provide further insight into the electrochemical behavior observed in the case of the trisradical complex.

4. Digital Simulations of Cyclic Voltammetry

The heterogeneous electron transfer reactions (Table S1) were derived using the ladder scheme outlined in Figure S6. The experimentally determined reduction potentials for each electron transfer reaction are also given in Table S1. Heterogeneous electron transfer rate constants were assumed to be much higher than those for the homogeneous chemical reactions.

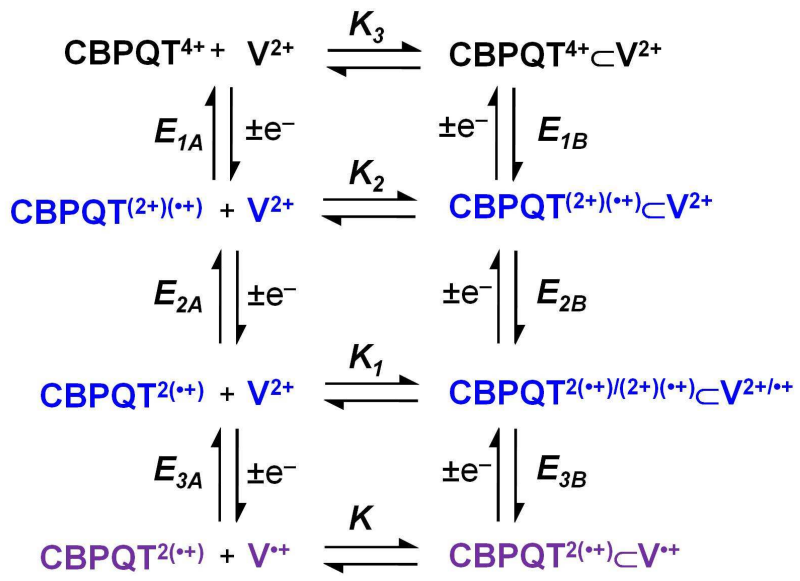

Figure S6. Square scheme mechanism for the formation of the trisradical complex from its fully oxidized components. The same scheme applies to the complexation of $CBPQT^{4+}$ and MV^{2+} by $CBPQT^{4+}$.

Table S1.Heterogeneous Electron Transfer Reactions		
	Reaction	***E*** **/ V**
1	$CBPQT^{4+} + MV^{2+} + e^{-} = CBPQT^{(2+)(\bullet+)} + MV^{2+}$	– 0.31
2	$CBPQT^{(2+)(\bullet+)} + MV^{2+} + e^{-} = CBPQT^{2(\bullet+)} + MV^{2+}$	– 0.31
3	$CBPQT^{2(\bullet+)} + MV^{2+} + e^{-} = CBPQT^{2(\bullet+)} + MV^{\bullet+}$	– 0.39
4	$CBPQT^{4+} \subset MV^{2+} + e^{-} = CBPQT^{(2+)(\bullet+)} \subset MV^{2+}$	– 0.00
5	$CBPQT^{(2+)(\bullet+)} \subset MV^{2+} + e^{-} = CBPQT^{2(\bullet+)/(2+)(\bullet+)} \subset MV^{2+/\bullet+}$	– 0.00
6	$CBPQT^{2(\bullet+)/(2+)(\bullet+)} \subset MV^{2+/\bullet+} + e^{-} = CBPQT^{2(\bullet+)} \subset MV^{\bullet+}$	– 0.24

The reduction potentials for MV^{2+} and V^{2+} are identical.

Table S2. Homogeneous Chemical Reactions				
	Reaction	K_{eq}	k_f (s^{-1})	k_b (s^{-1})
7	$CBPQT^{4+} \subset MV^{2+} = CBPQT^{4+} + MV^{2+}$	1.03×10^{8} *	1.0×10^{8} [b]	9.7×10^{-1}
8	$CBPQT^{4+} \subset MV^{\bullet+} = CBPQT^{4+} + MV^{\bullet+}$	2.64×10^{1} *	0.0	0.0
9	$CBPQT^{(2+)(\bullet+)} \subset MV^{\bullet+} = CBPQT^{(2+)(\bullet+)} + MV^{\bullet+}$	1.52×10^{-4} *	5.0×10^{3}	3.28×10^{7}
10	$CBPQT^{2(\bullet+)} \subset MV^{\bullet+} = CBPQT^{2(\bullet+)} + MV^{\bullet+}$	1.0×10^{-5} [a]	2.0×10^{2} [a]	2.0×10^{7}

*Values were calculated automatically by the software.
[a]Values determined from experiment.
[b]Assumed rate of formation constant based on ultra-fast decomplexation due to Coulombic repulsion. For more details, see ref. S6.

The homogeneous chemical reactions (Table S2) were also derived using the ladder scheme in Figure S6. Inputting the reduction potentials (Table S1) into the digital simulation software produced the equilibrium constants shown in Entries 7□9 listed in Table S2. The value of the rate constant k_f for entry 7 was assumed from theoretical calculations performed[6] on a similar system reported previously. Values for entry 10 in Table S2 were determined experimentally

from ITC and UV/Vis stopped-flow experiments. Table S3 lists the parameters that were used to conduct the CV experiments.

Table S3. CV Parameters				
E_{start} / V	E_{rev} / V	E_{end} / V	Area / cm^2	v / $V \cdot s^{-1}$
0.25	□1.5	0.25	0.071	VARIABLE

Species Parameters

Diffusion coefficients determined from ^{1}H NMR DOSY experiments for $CBPQT^{4+}$ and MV^{2+} were used when fitting the experimental to the simulated data. See Section 3 of the SI for more details.

5. X-Ray Crystallography

X-Ray diffraction data were collected on a Bruker Kappa diffractometer, equipped with a CuKα sealed-tube microsource and an APEX II CCD detector. Crystal data for [$CBPQT^{2(+\bullet)}\bullet 2PF_6$□$\subset MV^{+\bullet}\bullet PF_6$□] Crystal color: black. Crystal shape: cube. Crystal size: 0.10 x 0.09 x 0.09 mm. Crystal data for: $C_{36}H_{32}N_4 \subset C_{12}H_{14}N_2 \bullet 3(PF_6)$, $4(CH_3CN)$, M_r = 1306.03, monoclinic, space group *P*21/*n*, *a* = 9.702 (7), *b* = 14.786(9), *c* = 21.131(2) Å, *β* = 91.072(5)°, *V* = 3031.2(5) $Å^3$, *ρcalc* = 1.431 g cm^{-3}, *Z* = 2, *T* = 100(2) K, reflections collected = 4765, unique reflections = 4479, R_1 = 0.0492 [$F>4\sigma(F)$], wR_2 = 0.1313 for all data.

X-Ray diffraction data were collected on a Bruker Kappa diffractometer, equipped with a CuKα sealed-tube microsource and an APEX II CCD detector. Crystal data for [$CBPQT^{2(\bullet+)}\bullet 2PF_6$] Crystal color: black. Crystal shape: needle. Crystal size: 0.3 x 0.1 x 01 mm. Crystal data for: $C_{36}H_{32}N_4\bullet 2(PF_6)$, *Mr* = 810.60, orthorhombic, space group *PBAM*, *a* = 10.1423(5), *b* = 21.8630(10), *c* = 10.0569(5) Å, *V* = 2230.03(19) $Å^3$, *ρcalc* = 1.207, *Z* = 2, *T* = 100(2) K,

reflections collected = 1848, unique reflections = 1110, R_1 = 0.1020 [$F>4\sigma(F)$], wR_2 = 0.3127 for all data. Disordered solvent localized within the cyclophane could not be modeled adequately and the pass through method was employed.

6. Isothermal Titration Calorimetry

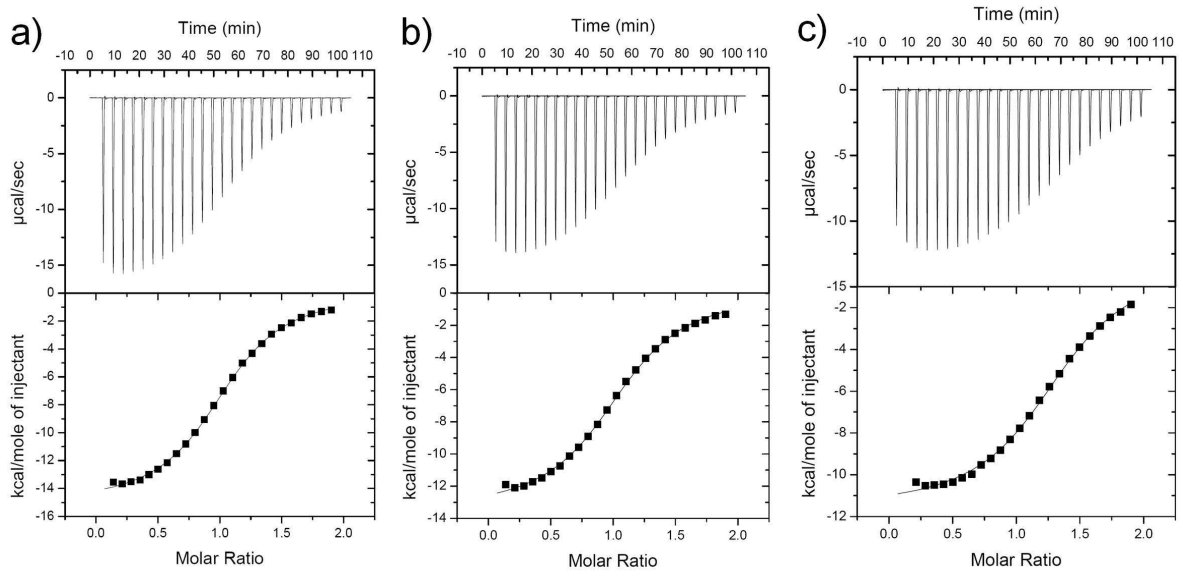

Figure S8. Isothermal titration calorimetry data for formation of the trisradical complex $CBPQT^{2(\bullet+)}\subset MV^{\bullet+}$. Each run was performed in MeCN at 298 K. The average of these three runs in addition to the experiment discussed in the main text, were used to calculate the binding constant *K*, the enthaplic (*ΔH)* and the entropic (*ΔS)* contributions to the binding free energy *ΔG*. The errors reported are the standard deviations acquired from these four experiments.

In a typical run, a 5 mM solution of $MV^{\bullet+}\bullet PF_6$ in MeCN is titrated into a 0.5 mM solution of $CBPQT^{2(\bullet+)}\bullet 2PF_6$ in MeCN. Solutions of radical cations were prepared based on the general procedure already outlined above in Section 2. All experiments were performed under the inert conditions of a glove box. The thermodynamic parameters obtained are an average over four individual runs, and the errors reported are calculated from the standard deviation of the four runs.

7. UV/Vis and Stopped-Flow UV/Vis Spectroscopy

Figure S9 shows the UV/Vis absorption spectra of the $CBPQT^{4+}$ ring and after reduction with zinc dust, its diradical dication $CBPQT^{2(\bullet+)}$. The spectrum of $CBPQT^{2(\bullet+)}$ is consistent with the monomeric forms of $BIPY^{\bullet+}$ radical cations.

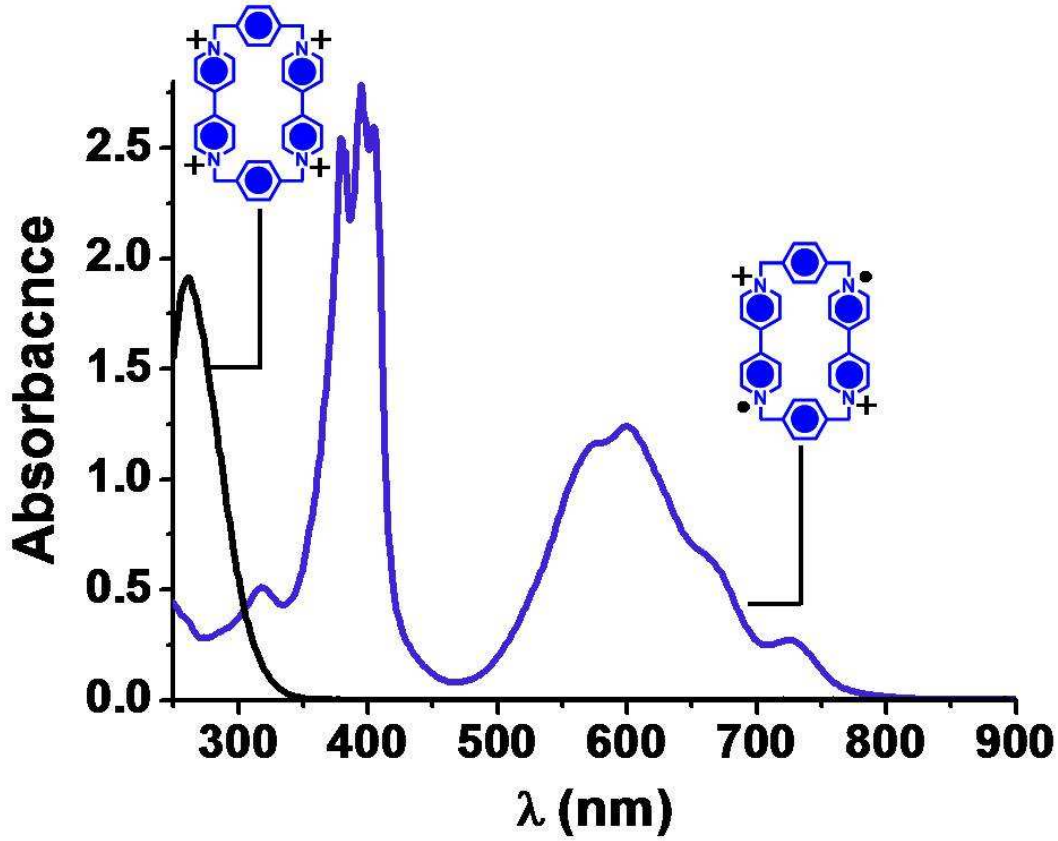

Figure S9. Disappearance of the $CBPQT^{4+}$ absorption band at 262 nm (ε^{262} = 4.38 x 10^4 M^{-1} cm^{-1}); Formation of a blue compound characterized by a set of vibronic bands centered at 395 nm (e^{395} = 6.39 x 10^4 M^{-1} cm^{-1}) and 599 nm (e^{599} = 2.84 x 10^4 M^{-1} cm^{-1}). No evidence of dimerization (absorption > 800 nm). Solvent: MeCN; $[CBPQT^{4+}]_0$ = 4.36 x 10^{-5} M; *T* = 25.0(2) °C; Reducing agent: activated Zn dust (30 mins to 1 h); *l* = 1 cm.

Figure S10 shows the UV/Vis absorption spectrum of MV^{2+} and, after being reduced with zinc dust, that of the $MV^{\bullet+}$ radical cation. The spectrum of $MV^{\bullet+}$ radical cation is consistent with its well-studied monomeric form.

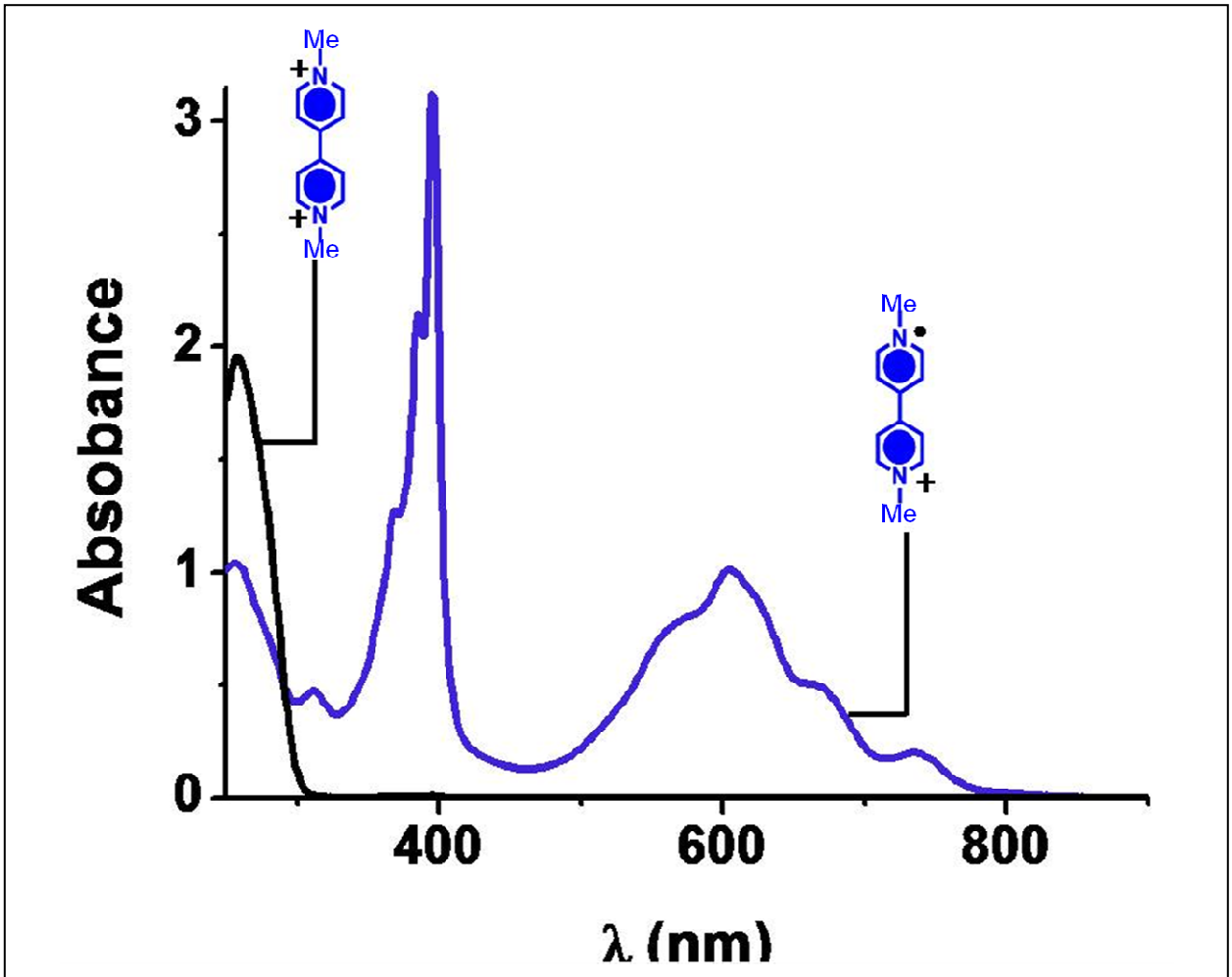

Figure S10. Decrease of the MV^{2+} absorption band at 257 nm (ε^{262} = 2.17 x 10^4 M^{-1} cm^{-1}); Formation of a blue compound characterized by a set of vibronic bands centered at 395 nm (e^{395} = 3.46 x 10^4 M^{-1} cm^{-1}) and 605 nm (e^{605} = 1.12 x 10^4 M^{-1} cm^{-1}). No evidence for dimerization or oligomerization processes (absorption > 800 nm). Solvent: MeCN; $[MV^{2+}]_0$ = 9.03 x 10^{-5} M; *T* = 25.0(2) ºC; Reducing agent: activated Zn dust (30 mins to 1 h); *l* = 1 cm.

Figure S11 shows the electronic spectra of $CBPQT^{2(\bullet+)}$, $MV^{\bullet+}$, and an electronic spectrum equivalent to adding two $MV^{\bullet+}$ spectra in order to compare to the $CBPQT^{2(\bullet+)}$ ring having two $BIPY^{\bullet+}$ units in its structure. The fact that the $CBPQT^{2(\bullet+)}$ ring has significantly higher extinction in the 600 nm region is one indication of the electronic coupling between its two $BIPY^{\bullet+}$ radical cation units, although they are too far apart to become dimerized (spin paired).

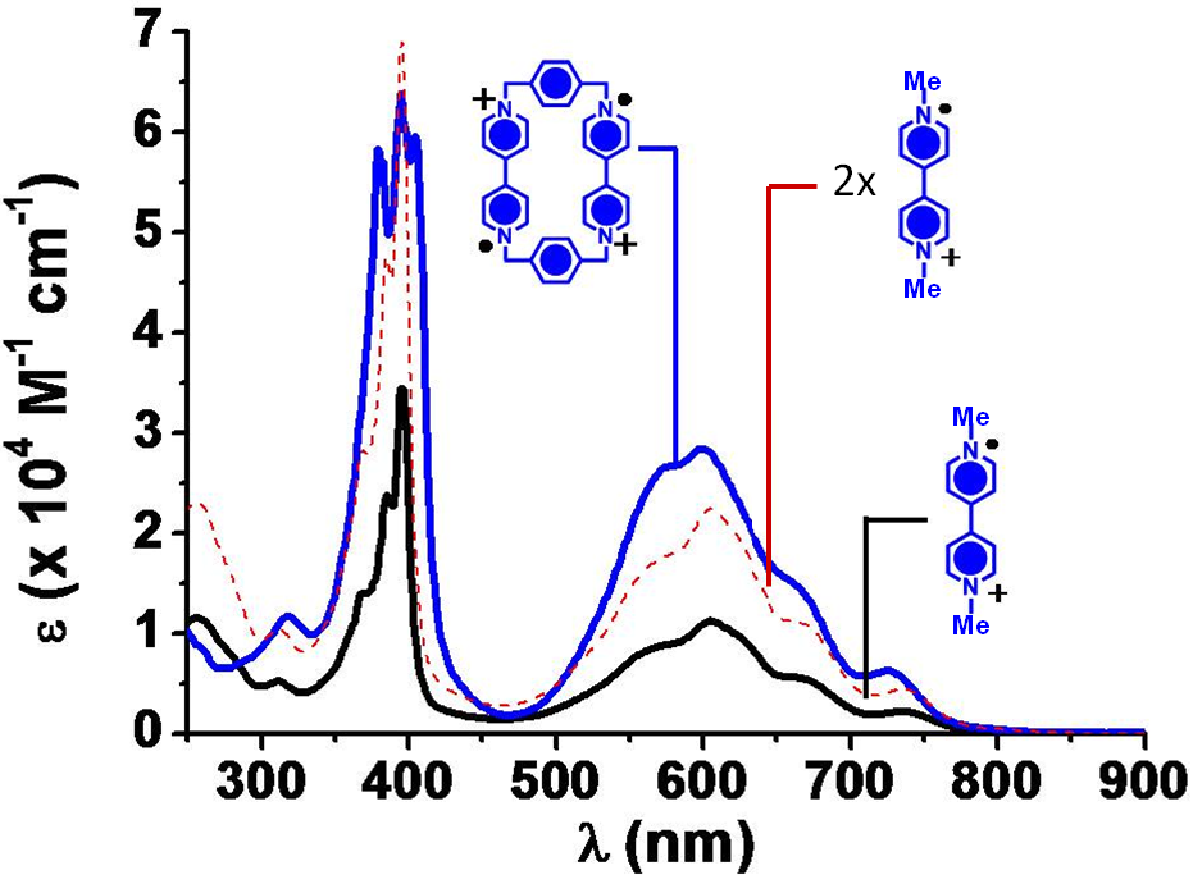

Figure S11. Electronic spectra of $CBPQT^{2(\bullet+)}$ and $MV^{\bullet+}$. Comparison of the electronic spectrum of $CBPQT^{2(\bullet+)}$ with the sum of the electronic spectra of two $MV^{\bullet+}$ indicates significant differences in agreement with strong electronic coupling in the ground state between the two chromophores. Solvent: MeCN; T = 25.0(2) ℃;

Figure S12 shows the electronic spectra of the trisradical complex $CBPQT^{2(\bullet+)}\subset MV^{\bullet+}$, and the sum of the electronic spectra of $CBPQT^{2(\bullet+)}$ and $MV^{\bullet+}$ recorded alone in solution. The fact that the extinction of the complex is larger in the 500 nm region, compared to the sum of the components, was exploited as a probe wavelength for monitoring the formation of the trisradical complex in the stopped-flow experiments.

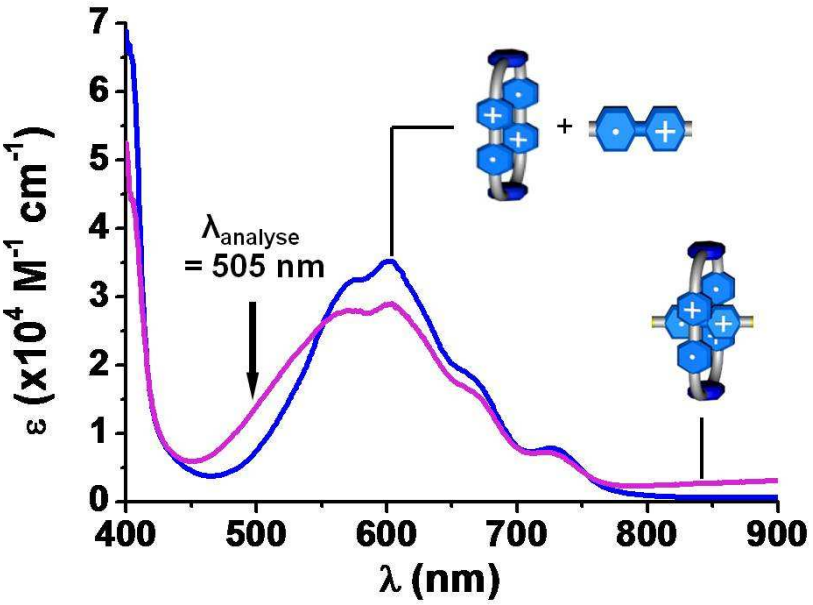

Figure S12. Electronic spectra of the sum of $CBPQT^{2(\bullet+)}$ and $MV^{+\bullet}$ (blue trace) and of $MV^{+\bullet}\subset CBPQT^{2(\bullet+)}$ (purple trace). Solvent: MeCN; *T* = 25.0(2) ℃. The largest differences in electronic spectrum occur at 505 nm and so was used to monitor complexation in the kinetic studies.

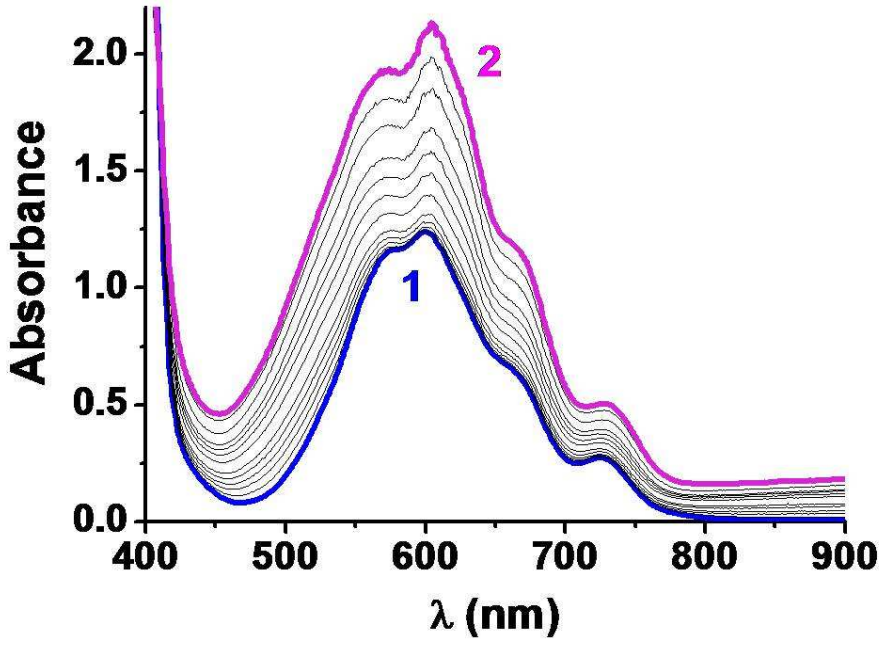

Figure S13. UV/Vis Absorption spectrophotometric titration of $CBPQT^{2+\bullet}$ by $MV^{+\bullet}$. Solvent: MeCN; *T* = 25.0(2) ℃; Reducing agent: activated Zn dust; *l* = 1 cm. (1) $[CBPQT^{2(\bullet+)}]_0$ = 4.36 x 10^{-5} M; (2) $[MV^{\bullet+}]_0$/ $[CBPQT^{2(\bullet+)}]_0$ = 4.38.

Figure S13 shows a spectrophotometric titration of $MV^{\bullet+}$ into a solution of $CBPQT^{2(\bullet+)}$. This data was used to calculate a binding constant (K) of 7.9 ± •10^4 M^{-1}, which agrees well with the value obtained from ITC experiments.

Supplementary References

S1 Sue, C.-H.; Basu, S.; Fahrenbach, A.; Shveyd, A. K.; Dey, S. K.; Botros, Y. Y.; Stoddart, J. F. *Chem. Sci.* **2010**, *1*, 119–125.

S2 Monk, P. M. S. *The Viologens: Physicochemical Properties, Synthesis and Applications of the Salts of 4,4'-Bipyridine*. John Wiley & Sons Ltd. New York, **1998**.

S3 Coskun, A.; Saha, S.; Aprahamian, I.; Stoddart, J. F. *Org. Lett.* **2008**, *10*, 3187–3190.

S4 Li, H.; Fahrenbach, A. C.; Dey, S. K; Basu, S.; Trabolsi, A.; Zhu, Z.; Botros, Y. Y.; Stoddart, J. F. *Angew. Chem. Int. Ed.* **2010**, *49*, 8260–8265.

S5 Smith, C. R. *Synlett* **2009**, 1522–1523.

S6 Kim, H.; Goddard III, W.A.; Jang, S.S.; Dichtel, W.R.; Heath, J.R.; Stoddart, J.F. *J. Phys. Chem. A* **2009**, *113*, 2136–2143.